Sustainable Aviation Fuels vs. Jet A-1: Experimental Insights into Laminar Burning Velocity and Minimum Ignition Energy

Hamamousse N.[1*], Brodu E.[1], Strozzi C.[2]*, Boust B.[1], Sotton J.[1] Bellenoue M.[1], C. Viguier[3]
[1] Institut Pprime, CNRS, ISAE-ENSMA
[2] Institut Pprime, CNRS, ISAE-ENSMA, Université de Poitiers
[3] Safran Helicopter Engines
Chasseneuil-du-Poitou, Nouvelle Aquitaine, France

1. Introduction

The global challenge of reducing carbon emissions and limiting global warming to 1.5°C by the end of the century has prompted intensified efforts to meet the Paris Agreement's goals, including peaking greenhouse gas (GHG) emissions by 2025 and reducing them about 43% by 2030 [3]. The aviation industry, contributing approximately 2.5% of global GHG emissions and 3.5 trillion dollars annually to the global economy [4], is at a critical juncture. Its dependence to conventional fossil fuels underscores the need for sustainable practices to balance economic growth with environmental responsibility [5]. Sustainable aviation fuels (SAFs) are a practical short- to medium-term decarbonization solution [6], given the current technological limitations of electrifying aircraft. The SAFs adoption targets for EU airports are 2% by 2025, 6% by 2030, and 20% by 2035, with a long-term goal of 70% by 2050 [8].

SAFs are classified as drop-in and non-drop-in fuels, with drop-in fuels easily integrating into existing systems without engine modifications [9]. Despite their advantages, SAFs face challenges such as limited availability, higher production costs, and slightly lower energy density than conventional Jet-A1 fuel [9,10]. SAFs, composed of renewable feedstocks, can reduce carbon emissions by up to 80% [9,10]. Their chemical structure, including linear paraffins, cycloparaffins, olefins, and aromatic compounds, influences key properties like freezing point, density, viscosity, and combustion behavior [11]. According to ASTM standards, SAFs can be blended with Jet-A1 and used without aircraft modifications [12].

Combustion parameters like laminar burning velocity (LBV), Markstein length (ML), and Minimum Ignition Energy (MIE) are essential for understanding SAFs performance and ignition safety. ML reflects flame stability, with positive values indicating stability and negative values signaling instability. Previous research conducted at Institut Pprime, has analyzed LBV and ML for kerosene and surrogates, offering insights into flame behavior under high temperatures and pressures [13-15].

In this study, experiments were conducted at Institut PPRIME as a part of the project VOLCAN, which focuses on the study of some alternative aviation fuels. In this study, Jet-A1 and three different types of SAFs are investigated. The first step of this study evaluates the LBV, ML, and MIE of three SAF types: i) Alcohol-to-Jet (ATJ), ii) Hydro processed Esters and Fatty Acids (HEFA), and iii) HEFA2 (a variant

Correspondence to: nadjet.hamamousse@ensma.fr

with added aromatics) under controlled conditions, at two pressures (0.1 MPa and 0.3 MPa) and two temperatures (400 K and 473 K). Equivalence ratio values varied from 0.7 to 1.5. Comparison with Jet-A1 was realized. In the second step, MIE experiments were conducted for fuel-lean mixtures at a fixed equivalence ratio (Φ = 0.7), at 473 K and 0.1 MPa. This extended abstract is structured into sections detailing experimental setup, results, and conclusions, providing critical data for advancing SAF technologies and achieving sustainable aviation goals.

2. Experimental Setup

Experiments were realized at Institut PPRIME in the framework of the VOLCAN project. Jet-A1 and three different types of SAFs were investigated. Their properties are summarized in Table.1. A stainless-steel spherical combustion chamber with an inner volume of 4.2 L and a diameter of 0.2 m was employed. Optical access for combustion visualization was provided by two ultraviolet (UV) quartz windows, each with a diameter of 0.07 m. The chamber was designed to be heated up to 470 K and operated at initial pressures up to 10 bar. Temperature control across the system was ensured by 24 cartridge heaters and heating tapes distributed along the chamber and feeding lines, while monitoring was carried out using four K-type thermocouples, positioned on the vessel and feeding lines. The chamber was evacuated prior to combustion initiation using a rotary-vane pump, reducing pressure below 350 Pa to eliminate residual gas. Pressure during combustion was measured by a piezoelectric dynamic pressure transducer (Kistler 6054AR) with a 0–300 bar range, protected by a 2 mm-thick silicone layer. Data capture was facilitated by an ICAM amplifier (Kistler Type 5073A). Ignition was achieved via electrical discharge between two tungsten electrodes with a diameter of 1 mm and a gap of 1 mm, generated by a transistorized coil igniter. Flame propagation was recorded with a high-speed Schlieren visualization system. High-definition images of the flame front were captured by a Photron FASTCAM SA5 camera at 7 kHz and 1,024 × 1,024-pixel resolution, using a collimated LED light source for illumination. Synchronization between the camera and pressure system was achieved using a TTL signal triggered by the ignition spark. The air-fuel mixture was prepared within the chamber, which is first evacuated, then flushed with air, and vacuumed again to ensure a controlled environment. Fuel was introduced using a micro-syringe, with precise monitoring of volume and pressure to prevent evaporation issues. Synthetic air (21% oxygen, 79% nitrogen by mole) is then added until the desired mixing pressure is achieved, ensuring accurate control of the fuel-to-air ratio. After stabilization, ignition at the chamber's center allowed the flame to expand spherically, enabling detailed combustion analysis.

Laminar flame speed and Markstein length are investigated using Schlieren visualization of flame propagation. A MATLAB program from a previous study is employed to analyze Schlieren images frame by frame, extracting the time-evolution of the flame radius, $R_f(t)$ [13-15]. The images are binarized to identify the flame edge, enabling calculation of the flame surface and the equivalent radius. The flame propagation speed, $S_b = \frac{dR_f}{dt}$ (1), and stretch rate, $\kappa = \frac{2}{R_f} S_b$ (2), are determined to extrapolate the unstretched laminar burning velocity S_b^0 and Markstein length $\mathcal{L}_b$ using Kelley and Law's model [16]. The model equation is : $\left(\frac{S_b}{S_b^0}\right)^2 ln\left(\frac{S_b}{S_b^0}\right)^2 = -\frac{2\,\mathcal{L}_b \kappa}{S_b^0}$. Then, the unstretched laminar burning velocity S_U^0 and Markstein length $\mathcal{L}_u$ are calculated by dividing S_b^0 and $\mathcal{L}_b$ by the ratio of burnt to unburnt gas densities, ρ_u/ρ_b, obtained through CANTERA software and thermodynamic data [17]. Thus, the unstretched laminar flame speed is: $S_u^0 = \frac{\rho_b}{\rho_u} S_b^0$

Table 1: Fuel properties

Fuel	Jet A1	HEFA	ATJ	HEFA2 (HEFA+aromatics)
average molecular formula	$C_{10,61}$ $H_{20,49}$	$C_{11,7}$ $H_{25,17}$	$C_{12,12}$ $H_{26,13}$ (C_{11}, C_{12}(+), C_{14})	$C_{11,26}$ $H_{20,63}$
Formula used to determine σ	$C_{10}H_{20}$	$C_{12}H_{26}$	$C_{12}H_{26}$	$C_{11}H_{22}$
average molar mass (g/mol)	147,81	165,57	171,57	155,75
mass % of heavy molecules (> 12 C)	16,40 %	40,27 %	15,83 %	31,43 %

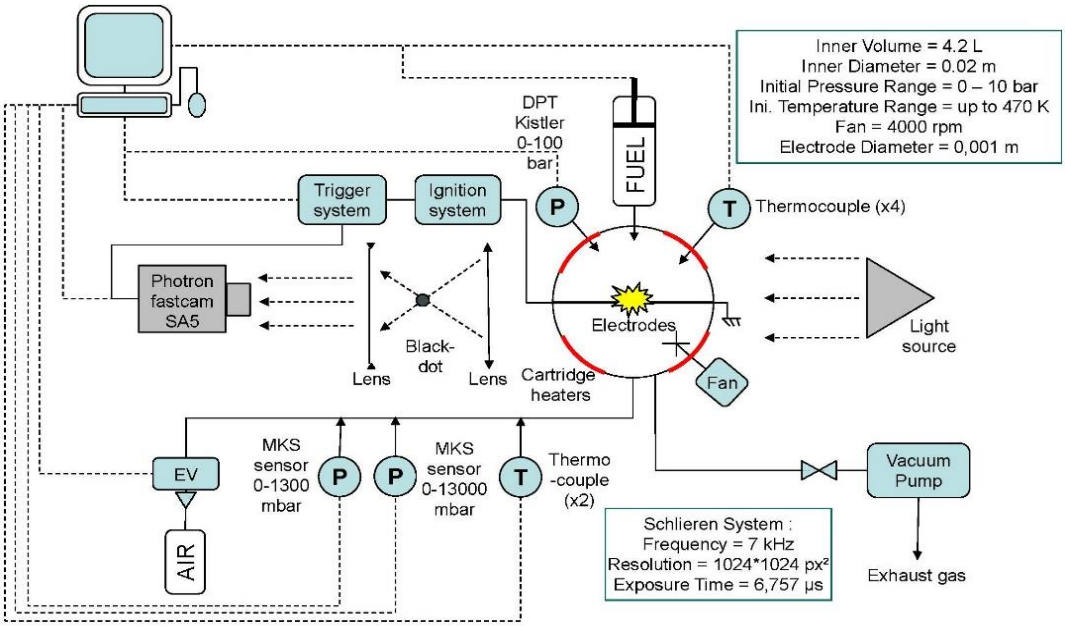

Figure 1: Schematic of the experimental setup.

4 Results

4.1. Laminar burning velocity

The results for the four fuels at an initial pressure of 1 bar and temperatures of 400 K and 473 K are summarized in Figure 2. The measurement uncertainty for the unstretched laminar flame speed (Su^0) is below 5 cm/s. The typical bell-shaped flame speed curves were observed, with relatively similar values for the fuels. However, ATJ fuel showed slightly lower flame speeds under rich conditions and was harder to ignite at 400 K. At higher pressure (3 bar, see Fig.3), Jet-A1 and HEFA2 exhibited better LBV performance with higher flame speeds, while ATJ had reduced speeds for richer mixtures. HEFA displayed much lower flame speeds across all equivalence ratios and caused soot deposits at equivalence ratios above 1.1. Limited data exists on flame velocity for long-chain hydrocarbons, but studies indicate that molecular structure significantly impacts flame speed[17]. Unsaturated hydrocarbons like alkynes and alkenes show the highest speeds, followed by cycloalkanes and alkanes, with longer chain lengths reducing flame speed [17]. HEFA2 and Jet-A1's higher flame speeds suggest aromatic compounds enhance combustion rate.

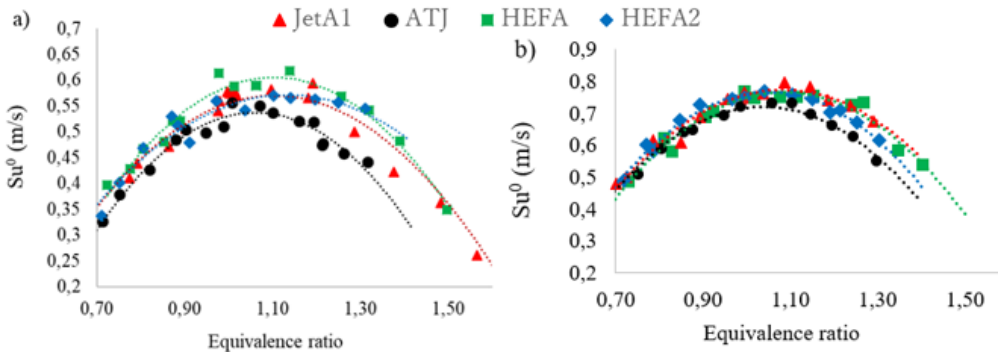

Figure 2: Laminar flame velocity Su^0 at P_0*=1 bar,* T_0*=400 K (a),* T_0*=473 K (b)*

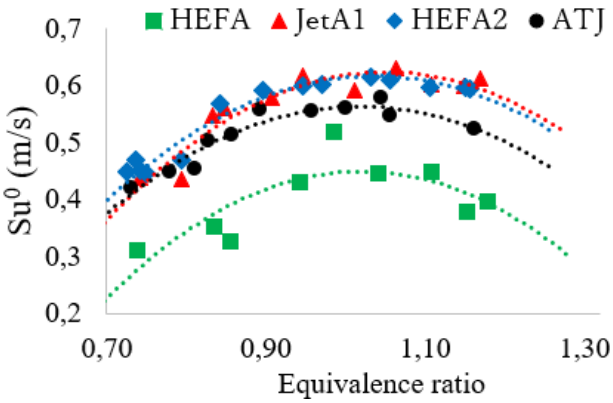

Figure 3: Laminar flame velocity Su^0 at P_0*=3 bar,* T_0*=473 K.*

The analysis of the impact of initial pressure and temperature on unstretched laminar flame velocity for different fuels across equivalence ratios show that the flame speed increases with temperature but decreases with pressure. Tests with Jet-A1 and HEFA from previous campaigns confirm that their flame velocities align with those of new samples, despite slight compositional variations in HEFA observed through chromatography. These variations do not affect flame speeds, but the reasons for the pressure-dependent decrease remain unclear.

4.2. Markstein length

The Markstein length reflects flame propagation stability. A positive Markstein length indicates that increased stretch reduces flame velocity, creating a feedback mechanism where disturbances at the flame front decrease stretch and stabilize the flame. This dynamics promotes stability by balancing flame dynamics and external influences. In contrast, a negative Markstein length amplifies disturbances, causing greater instability. Figure 4 shows Markstein length variations at P_0 = 1 bar for both temperatures, with all fuels following similar trends. A notable sign change near equivalence ratios of 1.3 highlights a threshold where flame dynamics shift. Thus, temperature has little to no significant influence on the Markstein length.

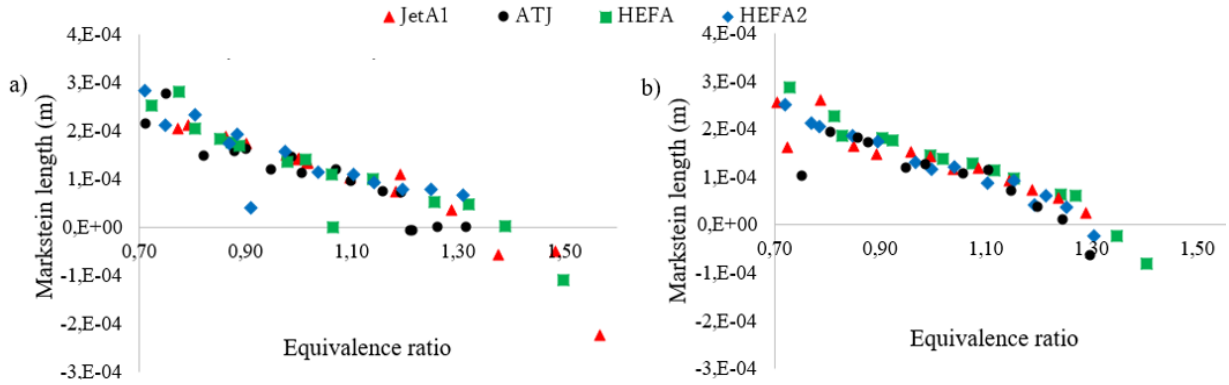

Figure 4: Markstein length versus the equivalence ratio for P_0=1 bar, T_0=400 K (a), T_0=473 K (b)

4.3. Minimum Ignition Energy (MIE)

Figure 5 illustrates the probability of ignition versus electrical energy for Jet-A1 and three SAFs, using the same spherical chamber and the data processing procedure described in [13]. Jet-A1 shows a significantly lower minimum ignition energy (MIE), approximately three times lower than ATJ, HEFA, and HEFA 2, which exhibit similar behaviors. Research by *Calcote et al*. indicates that MIE decreases from alkanes to alkenes and alkynes but increases with longer carbon chains [18]. Iso-alkanes have higher MIEs than n-alkanes, while cycloalkanes show lower MIEs, and aromatics have values comparable to n-alkanes. Jet-A1, that comprises cycloalkanes and shorter n-alkanes (C7), contrasts with ATJ, composed solely of iso-alkanes with C11 as the shortest chain. These compositional differences align with the observed MIE variations. The study, limited to a single equivalence ratio, highlights the need to test across multiple equivalence ratios for a complete understanding of ignition behaviors. While Jet-A1 achieves ignition reliability with less energy, HEFA, ATJ, and especially HEFA 2 require significantly higher energy to guarantee ignition.

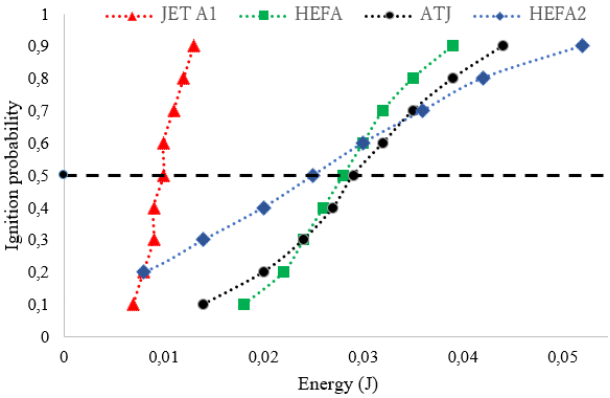

Fuel	MIE 50% (mJ)
Jet-A1	10
ATJ	29
HEFA	28
HEFA 2	25

Figure 5: Probability of ignition versus the discharge electrical energy at $\Phi = 0.7, T_0 = 473\ K$, and $P_0 = 1\ bar$

References

[1] Braun M., Grimme W., Oesingmann K. (2024). Pathway to net zero: Reviewing sustainable aviation fuels, environmental impacts and pricing. Journal of Air Transport Management, Volume 117. https://doi.org/10.1016/j.jairtraman.2024.102580.

[2] Ik J., Lau C., Wang Y. S., Ang T., Seo J.C.F., Khadaroo S.N.B.A., Chew J.J., Ng Kay Lup A., Sunarso J. (2024). Emerging technologies, policies and challenges toward implementing sustainable aviation fuel (SAF), Biomass and Bioenergy, Volume 186, 107277, https://doi.org/10.1016/j.biombioe.2024.107277.

[3] United Nations. Paris Agreement. 2015. Available online: https://unfccc.int/sites/default/files/english_paris_agreement.pdf (accessed on October 2024).
[4]. Hasan, M.A., Mamun, A.A., Rahman, S.M., Malik, K., Al Amran, M.I.U., Khondaker, A.N., Reshi, O., Tiwari, S.P., and Alismail, F.S. (2021). Climate change mitigation pathways for the aviation sector. Sustainability 13, 3656. https://doi.org/10. 3390/SU13073656.
[5] U.S. Department of Energy. Sustainable Aviation Fuel: Review of Technical Pathways. (2020). Available online: https://www. energy.gov/sites/prod/files/2020/09/f78/beto-sust-aviation-fuel-sep-2020.pdf (accessed on october 2024).
[6] Yoo, E., Lee, U., and Wang, M. (2022). Lifecycle greenhouse gas emissions of sustainable aviation fuel through a net-zero carbon biofuel plant design. ACS Sustain. Chem. Eng. 10, 8725–8732. https://doi.org/ 10.1021/ACSSUSCHEMENG.2C00977
[7] European Commission. (2020). *Aviation: Commission sets out a roadmap for the EU to become a global leader in sustainable aviation.*
[8] Quante, G., Bullerdiek, N., Bube, S., Neuling, U., and Kaltschmitt, M. (2023). Renewable fuel options for aviation – a System-Wide comparison of Drop-In and non-Drop-In fuel options. Fuel 333, 126269. https://doi.org/10.1016/J.FUEL.2022. 126269.
[9] F. Afonso, M. Sohst, C.M.A. Diogo, S.S. Rodrigues, A. Ferreira, I. Ribeiro, R. Marques, F.F.C. Rego, A. Sohouli, J. Portugal-Pereira, H. Policarpo, B. Soares, B. Ferreira, E.C. Fernandes, F. Lau, A. Suleman. (2023) Strategies towards a more sustainable aviation: a systematic review, Prog. Aerosp. Sci. 137, 100878, https://doi.org/10.1016/j.paerosci.2022.100878.
[10] A.H. Bhatt, Y. Zhang, A. Milbrandt, E. Newes, K. Moriarty, B. Klein, L. Tao. (2023). Evaluation of performance variables to accelerate the deployment of sustainable aviation fuels at a regional scale, Energy Convers. Manag. 275, 116441, https://doi.org/10.1016/j.enconman.2022.116441.
[11] ASTM, A. D7566-16b: Standard Specification for Aviation Turbine Fuel Containing Synthesized Hydrocarbons. Book of Standards, 5. ASTM A. Standard Specification for Aviation Turbine Fuel Containing Synthesized Hydrocarbons. 2016.
[12] Goh, B.H.H., Chong, C.T., Ong, H.C., Seljak, T., Katrasnik, T., Jozsa, V., Ng, J.H., Tian, B., Karmarkar, S., and Ashokkumar, V. (2022). Recent advancements in catalytic conversion pathways for synthetic jet fuel produced from bioresources. Energy Convers. Manag. 251, 114974. https://doi. org/10.1016/J.ENCONMAN.2021.114974.
[13] Le Dortz R. Strozzi C., Sotton J. and Bellenoue M. (2019). Premixture ignition of Jet-A kerosene and some of its surrogates in flowing conditions", 27th International Colloquium on the Dynamics of Explosions and Reactives Systems, (ICDERS 2019), Beijing (China) 28th July-2nd August 2019.
[14] Le Dortz R., Bellenoue M., Sotton J. and Strozzi C. (2020). Effects of temperature and pressure on laminar burning velocity of a commercial kerosene and some comprehensive surrogates ", *Fuel*, https://doi.org/10.1016/j.fuel.2020.119426
[15] Le Dortz R. Strozzi C., Sotton J. and Bellenoue M. (2019). Comparative study of laminar burning velocity measurement between confined and unconfined spherical flames methods for methane/air and n-decane/air premixed flames", 27th International Colloquium on the Dynamics of Explosions and Reactives Systems, (ICDERS 2019), Beijing (China) 28th July-2nd August 2019
[16] Kelley AP, Law CK. (2009). Nonlinear effects in the extraction of laminar flame speeds from expanding spherical flames. Comb. Flame 156:1844-1851.
[17] Goodwin DG, Moffat HK, Speth RL (2016). Cantera: An object-oriented software toolkit for chemical kinetics, thermodynamics, and transport processes. http://www.cantera.org, Version 2.2.1.
[18] H. F. Calcote, C. A. Gregory, Jr., C. M. Barnett, and Ruth B. Gilmer “Spark Ignition, Effect of Molecular Structure”, Ind. Eng. Chem. 1952, 44, 11.